Supplementary Information (SI) for Journal of Materials Chemistry C.

Assessing the Electronic and Optical Properties of Lanthanum Diselenide: a computational study – Supporting Information

Lanjing Huo[†] and Christopher N. Savory[*,†,‡]

[†]*Department of Chemistry, University College London, Christopher Ingold Building, London WC1H 0AJ, UK*

[‡]*Thomas Young Centre, University College London, Gower Street, London WC1E 6BT, UK*

E-mail: uccacns@ucl.ac.uk

Supplementary Note 1: Convergence of transport properties of $LaSe_2$

The accidental degeneracy in the valence band of $LaSe_2$, as mentioned in the main text, provides additional complications when converging the theoretical transport properties, which are highly sensitive to the band curvature, and thus to the density of k-points used. To improve the accuracy of predicted properties, codes that solve the Boltzmann transport equations using computational data allow the interpolation of the electronic eigenvalue data produced on the k-point mesh used in the original ab initio calculation to produce a denser grid of points for improved performance and faster convergence. With computed scattering rates, this issue can be even more crucial due to many of the rates having an inverse square dependenence on $\mathbf{q}$, demanding dense meshes. In the underlying ab initio calculations the accidental degeneracy of $LaSe_2$ is maintained along the E to A, E to C and E to D symmetry lines regardless of the k-mesh; when interpolated, however, this degeneracy is broken when the underlying k-point mesh contains an odd number of divisions along any given reciprocal lattice vector. As a result, attempts at direct convergence of the interpolated meshes are not possible as the trend in properties becomes entirely non-monotonic. To address this issue, we use a sufficiently-dense even-only k-point mesh of $10\times20\times10$ for the underlying ab initio electronic structure, and then check the convergence of the transport properties with respect to the increasingly-dense meshes interpolated from this point, given in Supplementary Figure S8.

Supplementary Note 2: Photovoltaic metrics

As described in the Computational Methods, two metrics are used to assess $LaSe_2$ as a photovoltaic absorber. The SLME metric was proposed by Yu and Zunger in 2012[1] as a low-cost metric for screening candidate photovoltaic absorbers that moves beyond the detailed

balance limit by attempting to account for forbidden and indirect band gaps, as well the actual absorption profile of a material. The former is accounted for using a factor f_r, which is the fraction of radiative electron-hole recombination. In the detailed balance limit, this factor is assumed to be unity, while in the SLME approach, it is given by $f_r = e^{-\Delta/k_\mathrm{B}T}$ where k_B is the Boltzmann constant and $\Delta = E_g^{da} - E_g$, the difference of the lowest energy direct-allowed optical gap and the fundamental band gap. This factor takes into account that in absorbers with indirect band gaps or optical transitions forbidden by crystal symmetry, a greater proportion of recombination is likely to be non-radiative, and the efficiency will be reduced from the detailed balance limit. Second, the photon absorptivity of the material is not assumed to be unity above the band gap, as in detailed balance, but, in the Beer-Lambert approximation, equal to $1 - e^{2\alpha(E)L}$, where $\alpha(E)$ is the calculated absorption coefficient and L the thickness of a film with a flat non-reflective front surface. This latter factor is then able to distinguish materials with "sharper" absorption profiles. Together, this allows an assessment of materials using calculable materials parameters.

The metric of Blank et al. noted drawbacks in the SLME approach:[2] firstly, a presumption of a flat non-reflecting front surface omits the impact of the refractive index. Secondly, that recombination losses are as likely from Shockley-Read-Hall recombination at defect centres in the material as from optical effects. In their approach, the refractive index is explicitly included within the calculation of the radiative saturation current density, and two possible models for the absorber's front surface are considered – the ideal flat surface as well as a diffuse-scattering Lambertian front surface. There is also no attempt to approximate non-radiative recombination – instead the internal quantum efficiency, Q_i, is employed as a user-determined factor to assess materials at different levels of non-radiative recombination, with $Q_i = 1$ returning the ideal radiative recombination of the detailed balance limit.

Supplementary Note 3: Scattering models

As discussed in the Computational Methods, the AMSET code[3] calculates mode-dependent scattering rates over the full Brillouin zone for three individual scattering processes: acoustic deformation potential (ADP) scattering, polar optical phonon (POP) scattering and ionized impurity (IMP) scattering. The matrix elements for each of the individual processes are given below for scattering from state $||n\mathbf{k}\rangle$ to state $||m\mathbf{k}+\mathbf{q}\rangle$.

Acoustic deformation potential scattering

$$g_{nm}^{\mathrm{ADP}}(\mathbf{k},\mathbf{q}) = \sqrt{k_{\mathrm{B}}T}\sum_{\mathbf{G}\neq-\mathbf{q}}\left[\frac{\tilde{\mathbf{D}}_{n\mathbf{k}}:\hat{\mathbf{S}}_{l}}{c_{l}\sqrt{\rho}}+\frac{\tilde{\mathbf{D}}_{n\mathbf{k}}:\hat{\mathbf{S}}_{t_1}}{c_{t_1}\sqrt{\rho}}+\frac{\tilde{\mathbf{D}}_{n\mathbf{k}}:\hat{\mathbf{S}}_{t_2}}{c_{t_2}\sqrt{\rho}}\right]\langle m\mathbf{k}+\mathbf{q}|e^{i(\mathbf{q}+\mathbf{G})\cdot\mathbf{r}}|n\mathbf{k}\rangle \quad (1)$$

wherein k_{B} is the Boltzmann constant, $\tilde{\mathbf{D}}_{n\mathbf{k}} = \mathbf{D}_{n\mathbf{k}} + \mathbf{v}_{n\mathbf{k}} \otimes \mathbf{v}_{n\mathbf{k}}$ (wherein $\mathbf{D}_{n\mathbf{k}}$ is the deformation potential tensor and $\mathbf{v}_{n\mathbf{k}}$ is group velocity of the state). $\hat{\mathbf{S}} = \hat{\mathbf{q}} \otimes \hat{\mathbf{u}}$ and is the unit strain associated with an acoustic mode (with l, t_1 and t_2 corresponding to the longitudinal and tranverse modes respectively) along $\hat{\mathbf{u}}$, the unit vector of phonon polarization.

Polar optical phonon scattering

$$g_{nm}^{\mathrm{POP}}(\mathbf{k},\mathbf{q}) = \left[\frac{\hbar\omega_{po}}{2}\right]^{\frac{1}{2}}\sum_{\mathbf{G}\neq-\mathbf{q}}\left(\frac{1}{\hat{\mathbf{n}}\cdot\epsilon_{\infty}\cdot\hat{\mathbf{n}}}+\frac{1}{\hat{\mathbf{n}}\cdot\epsilon_{\mathrm{s}}\cdot\hat{\mathbf{n}}}\right)^{\frac{1}{2}}\frac{\langle m\mathbf{k}+\mathbf{q}|e^{i(\mathbf{q}+\mathbf{G})\cdot\mathbf{r}}|n\mathbf{k}\rangle}{|\mathbf{q}+\mathbf{G}|} \quad (2)$$

wherein ϵ_{∞} and ϵ_{s} are the high frequency and static dielectric matrices respectively, and ω_{po} is the polar optical phonon frequency (obtained when each phonon mode is weighted by the dipole moment produced).

Ionized impurity scattering

$$g_{nm}^{\mathrm{IMP}}(\mathbf{k},\mathbf{q}) = \sum_{\mathbf{G}\neq-\mathbf{q}}\frac{n_i^{\frac{1}{2}}Ze}{\hat{\mathbf{n}}\cdot\epsilon_{\mathrm{s}}\cdot\hat{\mathbf{n}}}\frac{\langle m\mathbf{k}+\mathbf{q}|e^{i(\mathbf{q}+\mathbf{G})\cdot\mathbf{r}}|n\mathbf{k}\rangle}{|\mathbf{q}+\mathbf{G}|^2+\beta^2} \quad (3)$$

wherein e is the elementary charge, Z is the charge state of the impurity center, n_i is the concentration of ionized impurities (obtained via the targeted carrier concentration), and β

is the inverse screening length, given by:

$$\beta^2 = \frac{e^2}{\epsilon_s k_B T} \int \frac{\mathrm{dE}}{V} D(E) f(1-f) \tag{4}$$

where V is the volume of the unit cell, $D(E)$ the density of states and f is the Fermi-Dirac distribution.

Transport Properties

The matrix elements of the three scattering processes are combined to give a scattering lifetime $\tau_{n\mathbf{k}}$ for a given state. This can then be used to calculate the transport properties, for all state and k-points, via the spectral conductivity:

$$\Sigma_{\alpha\beta}(E) = \sum_n \int \frac{\mathrm{d}\mathbf{k}}{8\pi^3} \nu_{n\mathbf{k},\alpha} \nu_{n\mathbf{k},\beta} \tau_{n\mathbf{k}} \delta(E - E_{n\mathbf{k}}) \tag{5}$$

where α and β are Cartesian coordinates, and $E_{n\mathbf{k}}$ and $\nu_{n\mathbf{k}}$ are the energy and group velocity of band n at wavevector $\mathbf{k}$. The linearized Boltzmann transport equation is solved within the relaxation time approximation to give the conductivity and Seebeck coefficient via the Onsager transport coefficients.[4]

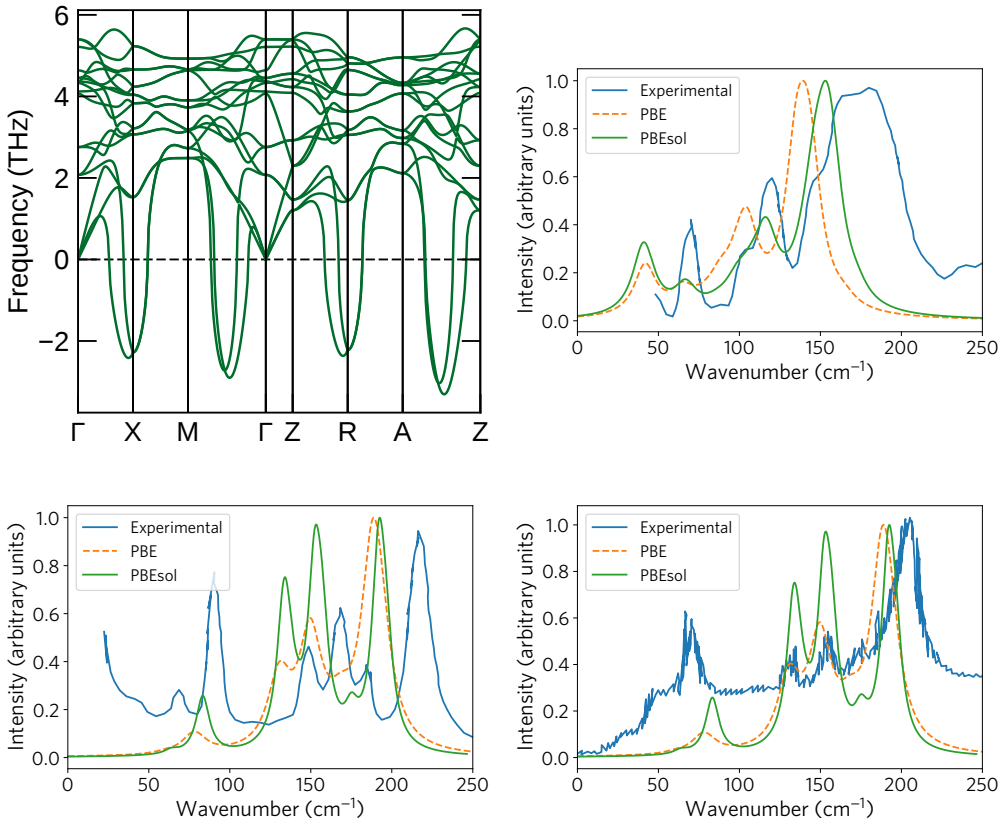

Figure S1: a) Phonon dispersion of $LaSe_2$ P4/mnm structure with PBEsol; b) Comparison of theoretical IR spectrum ($P2_1/c$) calculated with PBE and PBEsol with experimental powder IR from McMillan and co-workers; Comparison of theoretical Raman spectrum ($P2_1/c$) calculated with PBE and PBEsol with experimental powder Raman spectra from c) McMillan and co-workers (digitally extracted and reproduced)[5] and d) Gao et al.[6]

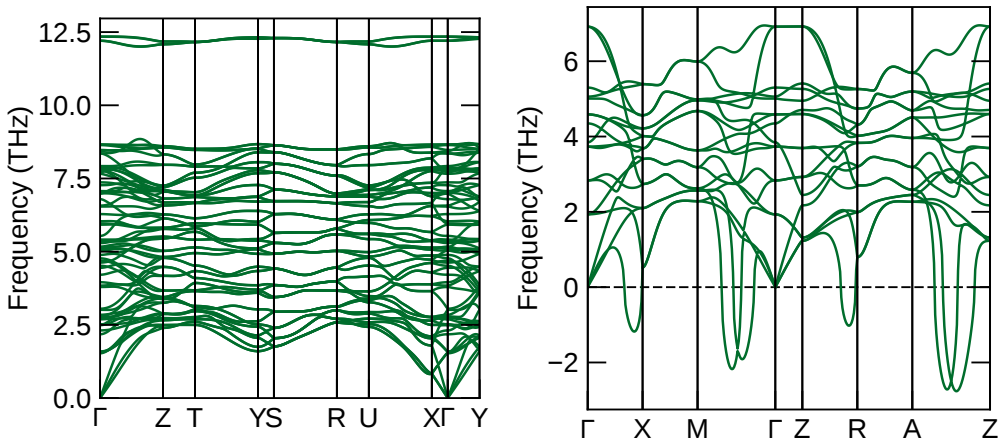

Figure S2: a) Phonon dispersion of LaS_2 P4/mnm structure b) P4/mnm structure of $LuSe_2$ calculated with PBEsol

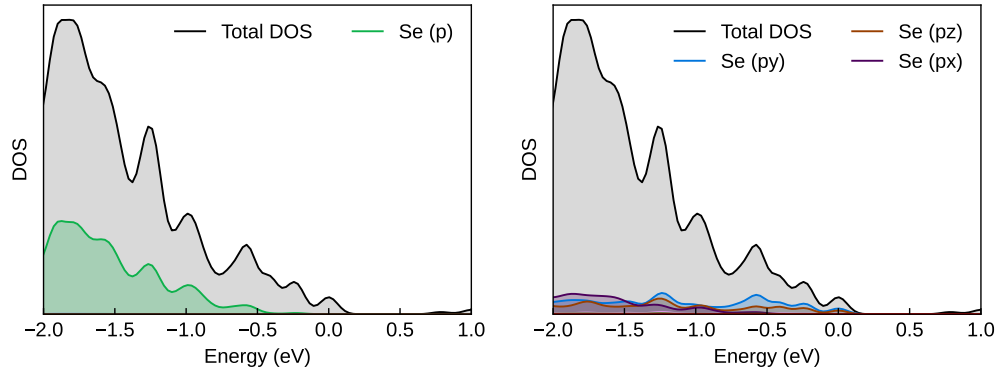

Figure S3: HSE06 partial densities of states for $P2_1/c$ structure of $LaSe_2$: a) Partial density of states for Se p states, considering atoms in La-Se bilayer only (Se^{2-}); b) Partial density of states for Se p states, considering atoms in Se-Se layer only (Se^{-}), with projections onto atomic m_l spherical harmonics – due to the orientation of the Se-Se bonds along the face diagonal of the cell, and the accidental degeneracy of the valence band maximum, the projections of p_x and p_y equally contribute, while p_z is only present lower in the valence band, demonstrating the anisotropic orbital contributions. Valence band maximum is set to 0 eV, and a Gaussian smearing of 0.15 eV added.

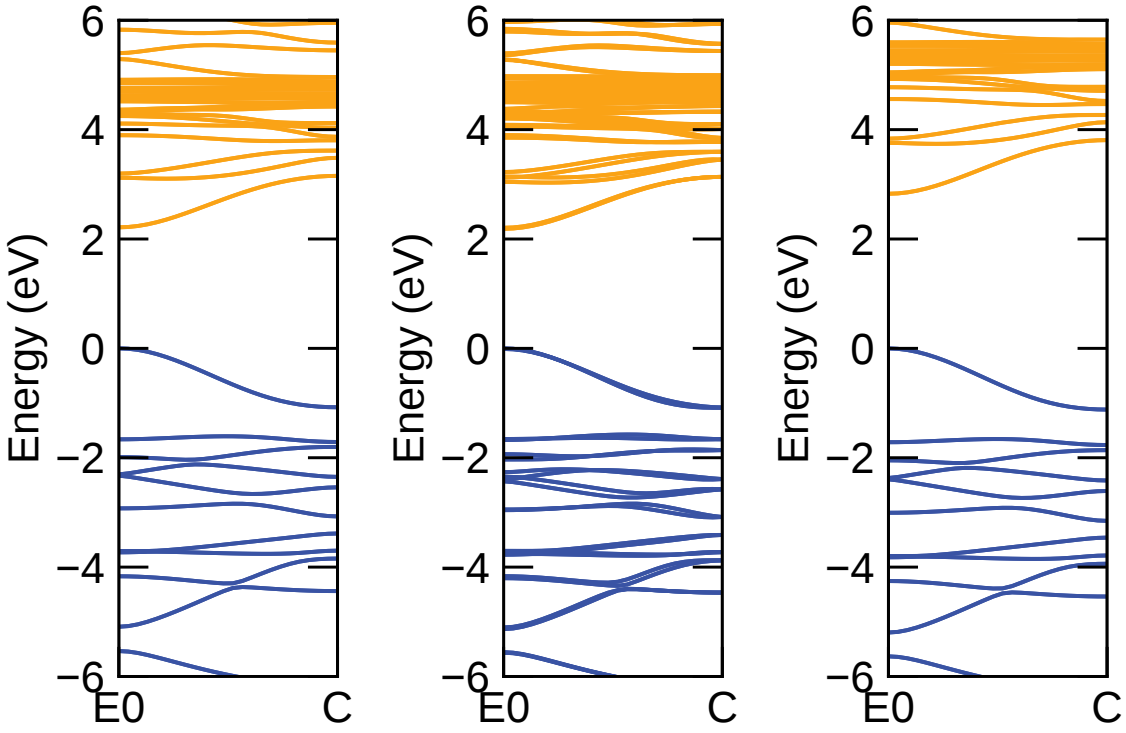

(a) (b) (c)

Figure S4: Electronic band structures calculated for $P2_1/c$ $LaSe_2$ using the following hybrid DFT functionals, along the E to C direction (correspondent to the z direction): a) HSE06 b) HSE06+SOC c) PBE0. All band structures are normalized such that the valence band maxmimum is set to 0 eV, with valence bands in blue and conduction bands in orange.

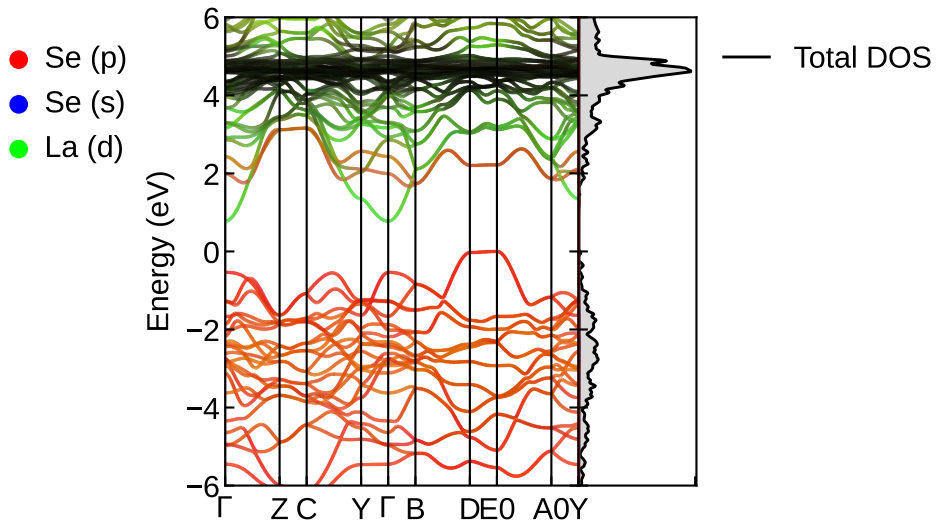

Figure S5: HSE06 band structure for $P2_1/c$ $LaSe_2$, with selected orbital projections projected as weights of the specified colours.

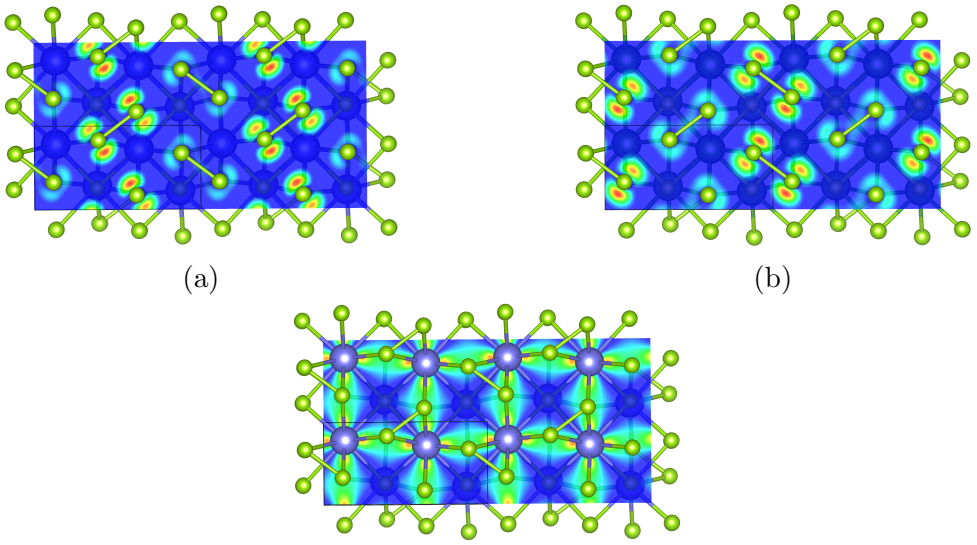

Figure S6: Partial charge densities at the a), b) degenerate valence band maxima (E) and c) conduction band minimum (Γ) of $LaSe_2$, calculated with HSE06 and projected onto a (100) Miller plane (the cell is also expanded to depict a 1×2×2 supercell). In a) and b) the plane intersects the plane of Se_2^{2-} dimers, in c) the plane intersects one of the planes of La atoms.

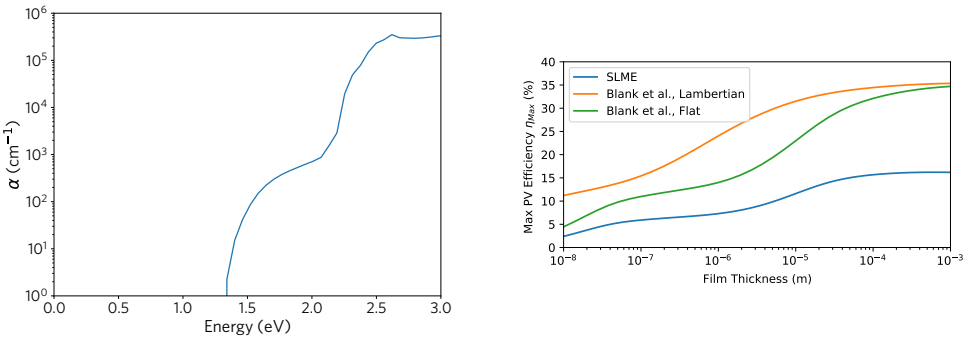

Figure S7: Calculated optical properties for P2$_1$/c $LaSe_2$: a) HSE06+SOC absorption coefficient, b) SLME and Blank et al. ($Q_i = 1$) metrics, given as a function of film thickness using HSE06+SOC dielectric and refractive index.

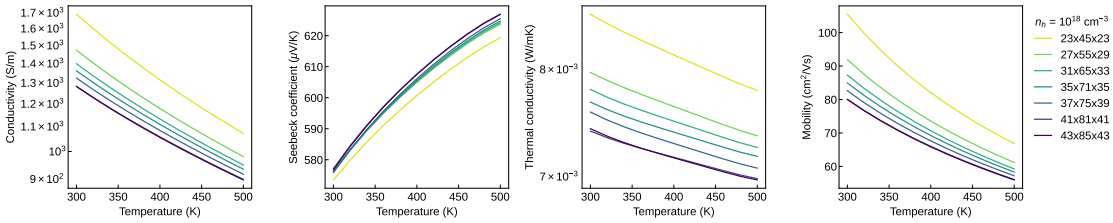

Figure S8: Convergence of transport properties with interpolated mesh points, plotted using the AMSET package.[3]

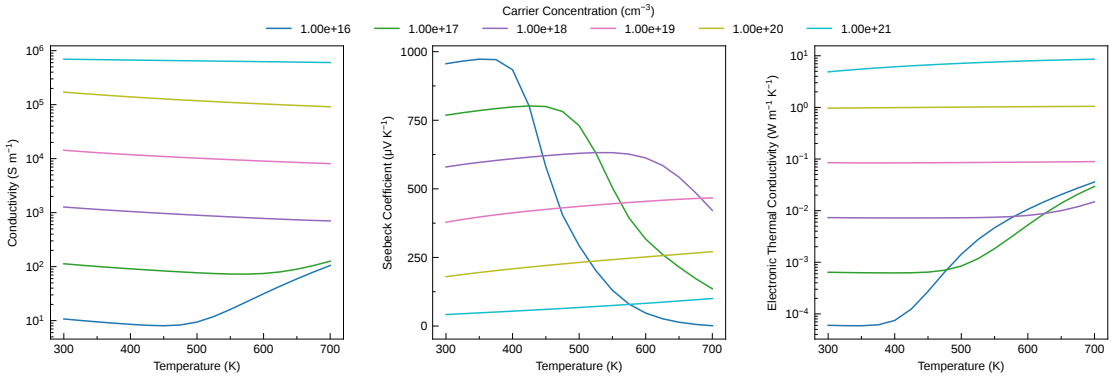

Figure S9: Predicted p-type electronic transport properties of $LaSe_2$ at a range of carrier concentrations and temperatures, plotted using the Thermoplotter package.[7] Inversion in the conductivity, Seebeck and electronic thermal conductivities at higher teperatures and low carrier concentrations arises when there is sufficient Fermi-Dirac population of the conduction band due to the low indirect band gap of $LaSe_2$.

References

(1) Yu, L.; Zunger, A. Identification of Potential Photovoltaic Absorbers Based on First-Principles Spectroscopic Screening of Materials. *Phys. Rev. Lett.* **2012**, *108*, 068701.

(2) Blank, B.; Kirchartz, T.; Lany, S.; Rau, U. Selection Metric for Photovoltaic Materials Screening Based on Detailed-Balance Analysis. *Physical Review Applied* **2017**, *8*, 024032.

(3) Ganose, A. M.; Park, J.; Faghaninia, A.; Woods-Robinson, R.; Persson, K. A.; Jain, A. Efficient calculation of carrier scattering rates from first principles. *Nature Communications* **2021**, *12*, 2222.

(4) Madsen, G. K.; Carrete, J.; Verstraete, M. J. BoltzTraP2, a program for interpolating band structures and calculating semi-classical transport coefficients. *Computer Physics Communications* **2018**, *231*, 140–145.

(5) Grzechnik, A.; Zheng, J. Z.; Wright, D.; william T. Petuskey,; Mcmillan, P. F. LaSe 2-x compounds: Vibrational and electrical properties. *Journal of Physics and Chemistry of Solids* **1996**, *57*, 1625–1634.

(6) Gao, G.; Tong, L.; Yang, L.; Sun, C.; Xu, L.; Xia, F.; Geng, F.; Xue, J.; Gong, H.; Zhu, J. A P-type mid-infrared transparent semiconductor $LaSe_2$ film with small hole effective mass and high carrier concentration. *Applied Physics Letters* **2021**, *118*, 261602.

(7) Spooner, K. B.; Einhorn, M.; Davies, D. W.; Scanlon, D. O. ThermoParser: Streamlined Analysis of Thermoelectric Properties. *Journal of Open Source Software* **2024**, *9*, 6340.